AFRL-RX-WP-JA-2016-0273

A ROTATIONAL AND AXIAL MOTION SYSTEM LOAD FRAME INSERT FOR IN SITU HIGH ENERGY X-RAY STUDIES (POSTPRINT)

Paul A. Shade, Jay C. Schuren, and Todd J. Turner
AFRL/RX

Basil Blank
PulseRay

Peter Kenesei, Kurt Goetze, Ulrich Lienert, and Jonathan Almer
Advanced Photon Source

Robert M. Suter and Jonathan Lind
Carnegie Mellon University

Joel V. Bernier, Shiu Fai Li, and Jonathan Lind
Lawrence Livermore National Laboratory

15 JULY 2015
Interim Report

(STINFO COPY)
AIR FORCE RESEARCH LABORATORY
MATERIALS AND MANUFACTURING DIRECTORATE
WRIGHT-PATTERSON AIR FORCE BASE, OH 45433-7750
AIR FORCE MATERIEL COMMAND
UNITED STATES AIR FORCE

REPORT DOCUMENTATION PAGE

Form Approved
OMB No. 0704-0188

1. REPORT DATE *(DD-MM-YY)*	2. REPORT TYPE	3. DATES COVERED *(From - To)*
15 July 2015	Interim	30 September 2014 – 15 June 2015

4. TITLE AND SUBTITLE
A ROTATIONAL AND AXIAL MOTION SYSTEM LOAD FRAME INSERT FOR IN SITU HIGH ENERGY X-RAY STUDIES (POSTPRINT)

5a. CONTRACT NUMBER
FA8650-14-D-5205-0001

5b. GRANT NUMBER

5c. PROGRAM ELEMENT NUMBER
62102F

6. AUTHOR(S)
1) Paul A. Shade, Jay C. Schuren, and Todd J. Turner – AFRL/RX
2) Basil Blank – PulseRay
(continued on page 2)

5d. PROJECT NUMBER
4349

5e. TASK NUMBER 0001

5f. WORK UNIT NUMBER
X0U5

7. PERFORMING ORGANIZATION NAME(S) AND ADDRESS(ES)
1) AFRL/RX
Wright-Patterson AFB, OH
45433-7750
2) PulseRay,
4583 State Route 414
Beaver Dams, NY 14812
(continued on page 2)

8. PERFORMING ORGANIZATION REPORT NUMBER

9. SPONSORING/MONITORING AGENCY NAME(S) AND ADDRESS(ES)
Air Force Research Laboratory
Materials and Manufacturing Directorate
Wright-Patterson Air Force Base, OH 45433-7750
Air Force Materiel Command
United States Air Force

10. SPONSORING/MONITORING AGENCY ACRONYM(S)
AFRL/RXCM

11. SPONSORING/MONITORING AGENCY REPORT NUMBER(S)
AFRL-RX-WP-JA-2016-0273

12. DISTRIBUTION/AVAILABILITY STATEMENT
Distribution Statement A. Approved for public release: distribution unlimited.

13. SUPPLEMENTARY NOTES
PA Case Number: 88ABW-2015-3613; Clearance Date: 15 July 2015. This document contains color. Journal article published in Review of Scientific Instruments, Vol. 86, No. 9, 8 Sep 2015.
The final publication is available at http://dx.doi.org/10.1063/1.4927855

14. ABSTRACT *(Maximum 200 words)*
High energy x-ray characterization methods hold great potential for gaining insight into the behavior of materials and providing comparison datasets for the validation and development of mesoscale modeling tools. A suite of techniques have been developed by the x-ray community for characterizing the 3D structure and micromechanical state of polycrystalline materials; however, combining these techniques with in situ mechanical testing under well characterized and controlled boundary conditions has been challenging due to experimental design requirements, which demand new high-precision hardware as well as access to high-energy x-ray beamlines. We describe the design and performance of a load frame insert with a rotational and axial motion system that has been developed to meet these requirements. An example dataset from a deforming titanium alloy demonstrates the new capability.

15. SUBJECT TERMS
High energy x-ray; 3D structure; micromechanical; polycrystalline materials; in situ mechanical testing; titanium alloy

16. SECURITY CLASSIFICATION OF:			17. LIMITATION OF ABSTRACT:	18. NUMBER OF PAGES	19a. NAME OF RESPONSIBLE PERSON (Monitor)
a. REPORT	b. ABSTRACT	c. THIS PAGE			Bill Song
Unclassified	Unclassified	Unclassified	SAR	12	19b. TELEPHONE NUMBER *(Include Area Code)* (937) 2551351

REPORT DOCUMENTATION PAGE Cont'd

6. AUTHOR(S)

3) Peter Kenesei, Kurt Goetze, Ulrich Lienert, and Jonathan Almer - APS

4) Robert M. Suter and Jonathan Lind - CMU

5) Joel V. Bernier, Shiu Fai Li, and Jonathan Lind - LLNL

7. PERFORMING ORGANIZATION NAME(S) AND ADDRESS(ES)

3) Advanced Photon Source
Argonne National Laboratory
9700 S Cass Ave, Lemont, IL 60439

4) Carnegie Mellon University
5000 Forbes Ave, Pittsburgh, PA 15213

5) Lawrence Livermore National Laboratory
7000 East Ave, Livermore, CA 94550

REVIEW OF SCIENTIFIC INSTRUMENTS **86**, 093902 (2015)

A rotational and axial motion system load frame insert for *in situ* high energy x-ray studies

Paul A. Shade,[1,a)] Basil Blank,[2] Jay C. Schuren,[1,b)] Todd J. Turner,[1] Peter Kenesei,[3] Kurt Goetze,[3] Robert M. Suter,[4] Joel V. Bernier,[5] Shiu Fai Li,[5,c)] Jonathan Lind,[4,5] Ulrich Lienert,[3,d)] and Jonathan Almer[3]

[1]*Materials and Manufacturing Directorate, Air Force Research Laboratory, Wright-Patterson AFB, Ohio 45433, USA*
[2]*PulseRay, Beaver Dams, New York 14812, USA*
[3]*Advanced Photon Source, Argonne National Laboratory, Argonne, Illinois 60439, USA*
[4]*Carnegie Mellon University, Pittsburgh, Pennsylvania 15213, USA*
[5]*Engineering Directorate, Lawrence Livermore National Laboratory, Livermore, California 94550, USA*

(Received 12 July 2015; accepted 22 July 2015; published online 8 September 2015)

High energy x-ray characterization methods hold great potential for gaining insight into the behavior of materials and providing comparison datasets for the validation and development of mesoscale modeling tools. A suite of techniques have been developed by the x-ray community for characterizing the 3D structure and micromechanical state of polycrystalline materials; however, combining these techniques with *in situ* mechanical testing under well characterized and controlled boundary conditions has been challenging due to experimental design requirements, which demand new high-precision hardware as well as access to high-energy x-ray beamlines. We describe the design and performance of a load frame insert with a rotational and axial motion system that has been developed to meet these requirements. An example dataset from a deforming titanium alloy demonstrates the new capability. [http://dx.doi.org/10.1063/1.4927855]

I. INTRODUCTION

There is a great deal of interest within the materials community to develop mesoscale modeling tools which are sensitive to the underlying microstructure. For example, adoption of an integrated computational materials engineering (ICME) approach to design of structural components is dependent on such a capability.[1–6] Development of trusted microstructure-sensitive deformation models may provide improved predictions of materials behavior, e.g., strength and damage resistance, enabling structural materials to be used more effectively and efficiently. While development of mesoscale models has been a major thrust of the materials community for several decades, these models have lacked the necessary multi-scale experimental validation, thus precluding design engineers from adopting them due to unacceptable risk factors. Looking forward, advanced materials characterization methods are positioned to play a critical role in the validation and future development of mesoscale models and the long term goal of transitioning such modeling tools to the design community.[5–20]

One particular suite of experimental techniques that promises to be extremely fruitful in this endeavor is known as high energy diffraction microscopy (HEDM) or three-dimensional x-ray diffraction (3DXRD).[6,21–23] These techniques utilize high energy monochromatic synchrotron radiation and area detectors in transmission geometry to collect diffracted x-rays as a function of sample rotation. This combination allows individual grain information from ~mm^3 volumes of polycrystalline materials to be determined non-destructively. When combined *in situ* with mechanical testing techniques, HEDM (or 3DXRD) offers a powerful tool to evaluate the internal structure and micromechanical state of a deforming material. To date, this collection of methods have largely been thought of as individual techniques, including far field HEDM (ff-HEDM) to measure the average elastic strain tensor of individual grains (stress tensor with known elastic stiffness matrix)[24–27] and near field HEDM (nf-HEDM) to map the structure and local crystallographic orientation within and between grains.[21,28,29] While the individual techniques are valuable on their own, the concurrent application of nf-HEDM, ff-HEDM, and others such as absorption micro-computed tomography (μ-CT) for mapping the structure of voids, cracks, and/or inclusions which may be present,[30] can provide incredibly rich datasets from which to develop and validate microstructure sensitive materials models.

The key factor that has restricted the collection of such integrated multimodal HEDM datasets *in situ* with traditional mechanical testing equipment is the stringent set of mechanical and geometrical requirements placed on the experimental setup. The requirements include precisely (≤0.1° precision) rotating a specimen over a range of 180° or more while simultaneously applying a mechanical load under known and controllable boundary conditions. Furthermore, the apparatus itself must not obstruct the incident, transmitted or diffracted x-ray signals and must allow the near field detector to be as close as 5 mm downstream of the specimen. In this paper, we describe a rotational and axial motion system (RAMS)[31]

a)Author to whom correspondence should be addressed. Electronic mail: paul.shade.1@us.af.mil
b)Present address: Nutonian, Inc., Somerville, Massachusetts 02144, USA.
c)Present address: Human Diagnosis Project, San Francisco, California 94110, USA.
d)Present address: DESY, Photon Science, Hamburg, Germany.

that we have developed to enable the concurrent application of high energy x-ray methods (ff-HEDM, nf-HEDM, μ-CT, and others) while conducting a conventional tensile or compressive loading experiment *in situ*.

II. DESIGN

The promise of advanced *in situ* characterization has inspired the development of a variety of complex experimental hardware at x-ray and neutron beamline facilities, each developed to accommodate a specific set of experimental requirements for the particular application. One solution for rotation of a sample with *in situ* mechanical testing has been to attach a load frame to the top of a rotation stage.[32–35] This solution is not practical for the current experimental requirements, as the location of the near field detector (~5 mm from the specimen) would limit the rotation range of the load frame to a small angular window beyond which the support columns would cause interference. At the same time, simple *ad hoc* arrangements have demonstrated the possibility and value of *in situ* loading that is compatible with near field measurements.[5,36,37] A more elegant solution is to rotate the specimen grips of a general purpose load frame synchronously while the rest of the load frame remains stationary;[38,39] this has the advantage of allowing complete rotation about the loading axis while also allowing more sophisticated loading control modes.

Using this approach, we have designed and constructed a RAMS device that is configured to mount within a conventional mechanical load frame. A schematic of the experimental setup is shown in Figure 1, where the RAMS device is shown inserted into a servohydraulic MTS model 858 load frame at the high energy beamline 1-ID-E at the Advanced Photon Source (APS), Argonne National Laboratory. An important design consideration was that the load frame insert be robust enough to safely deform specimens with hundreds of grains or more in a cross section; therefore, the RAMS device was designed around 1.0×1.0 mm^2 cross section samples and maximum axial loads of ±2000 N. The weight of the RAMS load frame insert is approximately 73 Kg, and the dimensions are approximately 436 mm × 270 mm × 731 mm (width × depth × height) when a sample is inserted (the upper half of the RAMS device can travel vertically through a range of 90 mm to enable sample insertion). Loads are applied with the load frame and transferred through the RAMS device to the sample. At the same time, the RAMS device rotates the sample about the loading axis in either discrete steps or continuously. Figure 1 also shows the x-ray beam path and near field and far field x-ray detectors. In Secs. II A–II C, we describe the

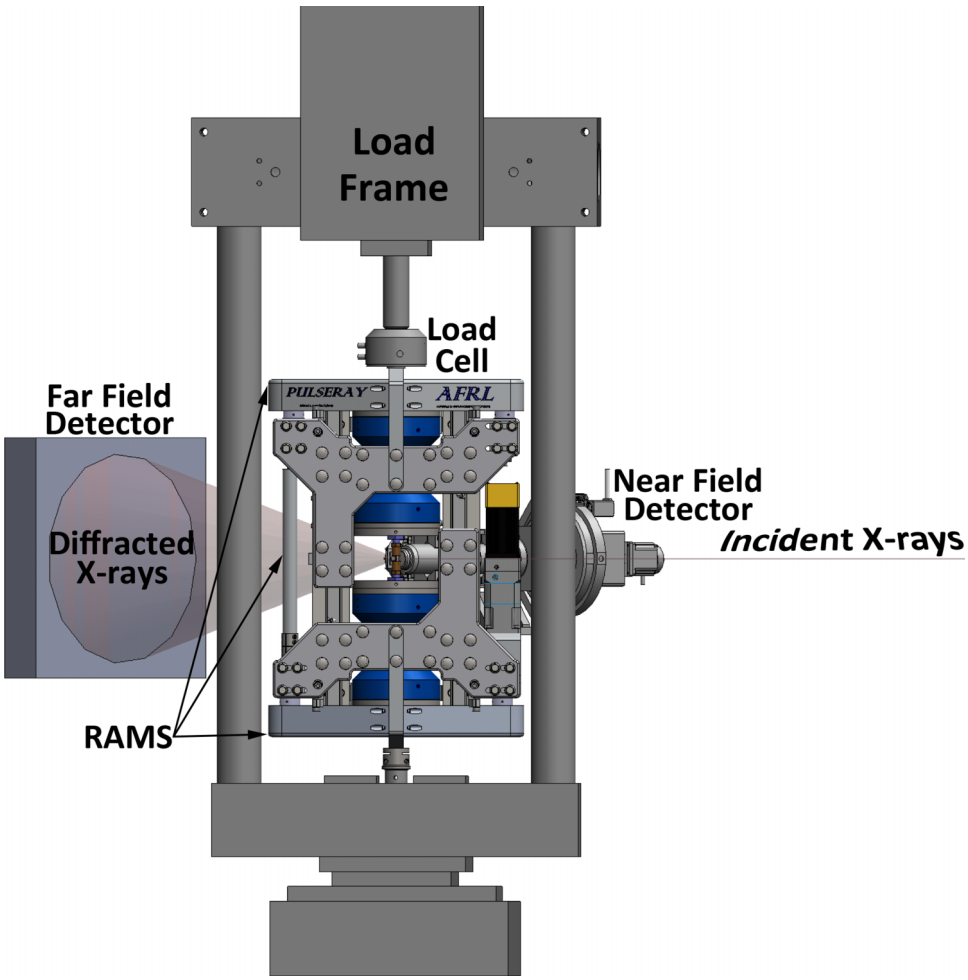

FIG. 1. Schematic of a setup utilized at APS 1-ID for high energy diffraction microscopy (HEDM) experiments. A rotational and axial motion system (RAMS) load frame insert is shown inserted into a conventional load frame along with near field and far field detectors. The loading axis is vertical, and the specimen and specimen grips rotate about the loading axis while the rest of the setup remains stationary. See Figures 2 and 3 for more detailed views.

various design criteria for the device and the corresponding design aspects that were utilized to meet them.

A. Rotation

The primary design constraint was to enable continuous rotation of the sample while independently and simultaneously applying an axial load. The radial and axial error motions (e.g., eccentricity and wobble) during rotation of a sample that has been centered on the rotation axis must be minimized.[40,41] These errors will lead to uncertainties in the HEDM measurements,[27,42] and potentially information that is missed altogether. The latter situation may occur when using a line focused (~few μm) x-ray beam if the rotation axis is not orthogonal to the line focus. At the same time, the system must be designed to remain rigid against the expected axial and non-axial loads.[43,44]

The solution chosen for this application involves a series of air bushings and air bearings that have been configured as combined air bushing/bearing spools. Separate upper and lower rotation stages, which are connected by a coupled drive shaft, are each comprised of two such spools. The air bushings and air bearings act to minimize the radial and axial error motions during rotation, respectively. A detailed schematic of the RAMS device with labeled components is presented in Figure 2.

The air bushing/bearing spools were initially aligned by utilizing a potting method, where an alignment shaft was threaded through all four spools simultaneously and subsequently their position was locked in place with an epoxy, after which the alignment shaft was removed and the air bushing shafts and air bearing plates, as shown in Figure 2, were installed. The alignment shaft, air bushing shafts, and air bearing plates were all manufactured with sub-micrometer precision. Subsequent calibration experiments involving an alignment pin and a dial indicator confirmed that the radial error motion was sub-micrometer, which is below the measurable resolution of the HEDM techniques. As mentioned earlier, the system was designed for maximum axial sample loads of ±2000 N. Accounting for the weight of the machine as well as potential load frame control mishaps, the air bushing/air bearing sub-system is designed for a maximum axial load of ±4400 N. Radially, the system was designed to withstand 50% of the maximum sample axial load, i.e., ±1000 N.

Rotation is accomplished through a servomotor, gear reducer, spline coupling drive shaft, and two timing belts. The spline coupling drive shaft allows the single servomotor to rotate the two stages synchronously and includes a preloaded linear ball spline which enables torque to be transferred to both the upper and lower rotation stages despite the fact that their vertical separation changes (along the tensile axis) throughout an experiment. Use of a single rotation motor was strongly preferred in this initial design as it eliminated the controls challenge of synchronizing the operation of the upper and lower rotation stages. This is critical in order to eliminate torsional loading of the specimen, which could lead to large

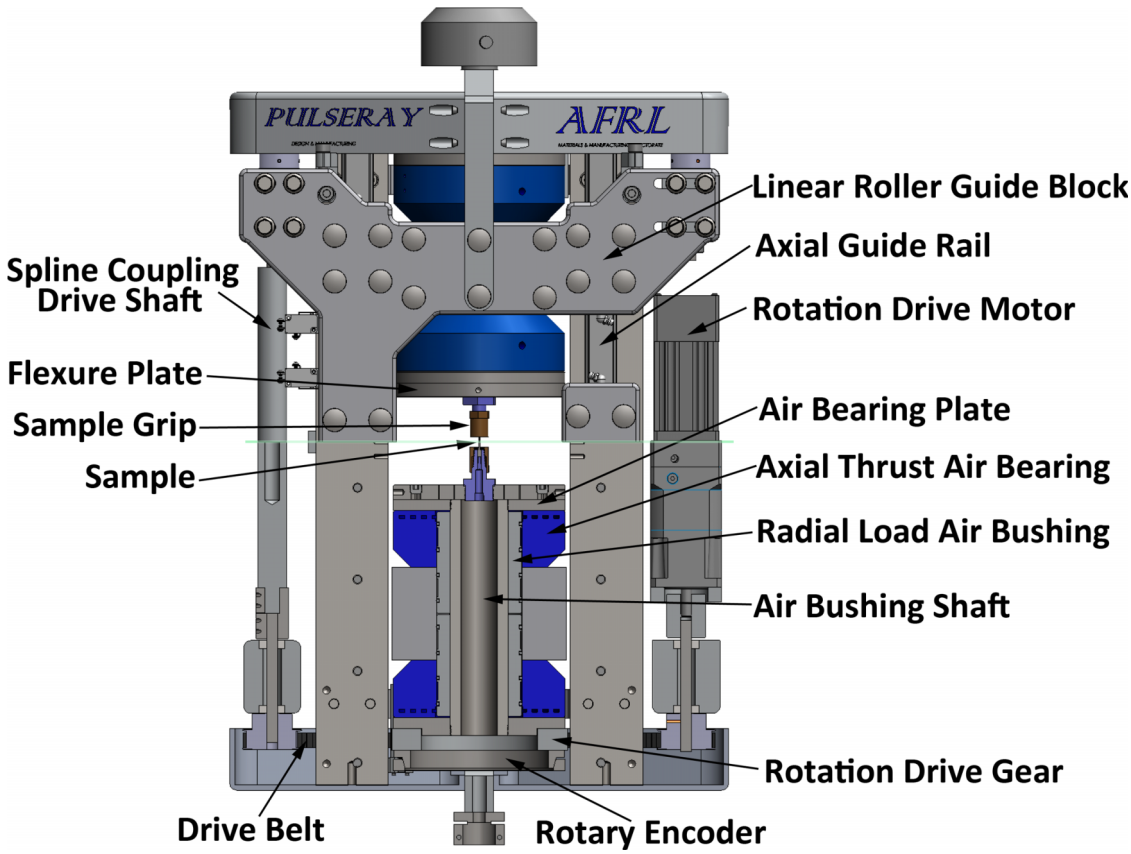

FIG. 2. Detailed schematic view of the RAMS load frame insert with various components labeled. The portion of the drawing below the light green line is a section view showing the internal details.

stresses for the typical sample cross sections used in HEDM experiments (~1 mm^2). The rotation position is monitored with a pair of rotary encoders. With this setup, the rotation precision is better than 0.1° at a maximum rotation rate of 10°/s. Future implementations of this device will utilize metallic gears rather than timing belts, as well as an optimized gear ratio, rotary encoder, and rotary encoder read head, which should enable improved precision at higher rotation rates.

B. Coaxial translation and alignment

Another critical design constraint was the coaxiality of the upper and lower rotation stages, as any deviations would impart bending stresses on the sample during rotation. The potting method used to align the upper and lower rotation stages was described in Section II A. This alignment was maintained during tension/compression testing through the use of an axial guide rail and linear roller guide block, as shown in Figure 2. This design utilized linear roller bearings to ensure that the vertical translation axis (tensile axis) of the upper rotation stage remained parallel to the coaxial rotation axes of the two rotation stages.

A related requirement was for the upper and lower sample grips, which, respectively, are attached to the upper and lower rotation stages, to be aligned such that the center of a sample mounted within the grips would be on the center of the rotation axis. The reasons for this are twofold. First, the center of the sample must be near the rotation axis so that a region of interest within the sample does not rotate out of the field of view (defined by the beam width of ~1.5 mm) during a measurement. Second, and perhaps more important, the centerlines of the upper and lower sample grips must be coaxial with each other in order to prevent non-axial loading of the sample during sample installation. Again, sample cross sections are typically 1 mm^2 or less, so small loads can lead to large stresses. The specimen tolerances in the grip region are relatively tight (±12.5 μm) to ensure proper grip force and repeatable position, so the alignment precision must be on the scale of a few micrometers or less. This was accomplished through the use of a flexure plate design,[45,46] as shown in Figures 2 and 3.

The flexure plates were constructed by machining a series of channels, effectively producing an array of springs creating two orthogonal adjustment directions within the plane of the plate (orthogonal to the tensile axis), as can be seen in Figure 3. The design challenge for optimizing the stiffness of the flexure plate in the adjustment directions was to balance the opposing objectives of being as stiff as possible (in order to apply rigid boundary conditions for a tension/compression test), while maintaining sufficient compliance in order to practically be able to make the necessary translational adjustments. The chosen solution was to design for a relatively rigid translational

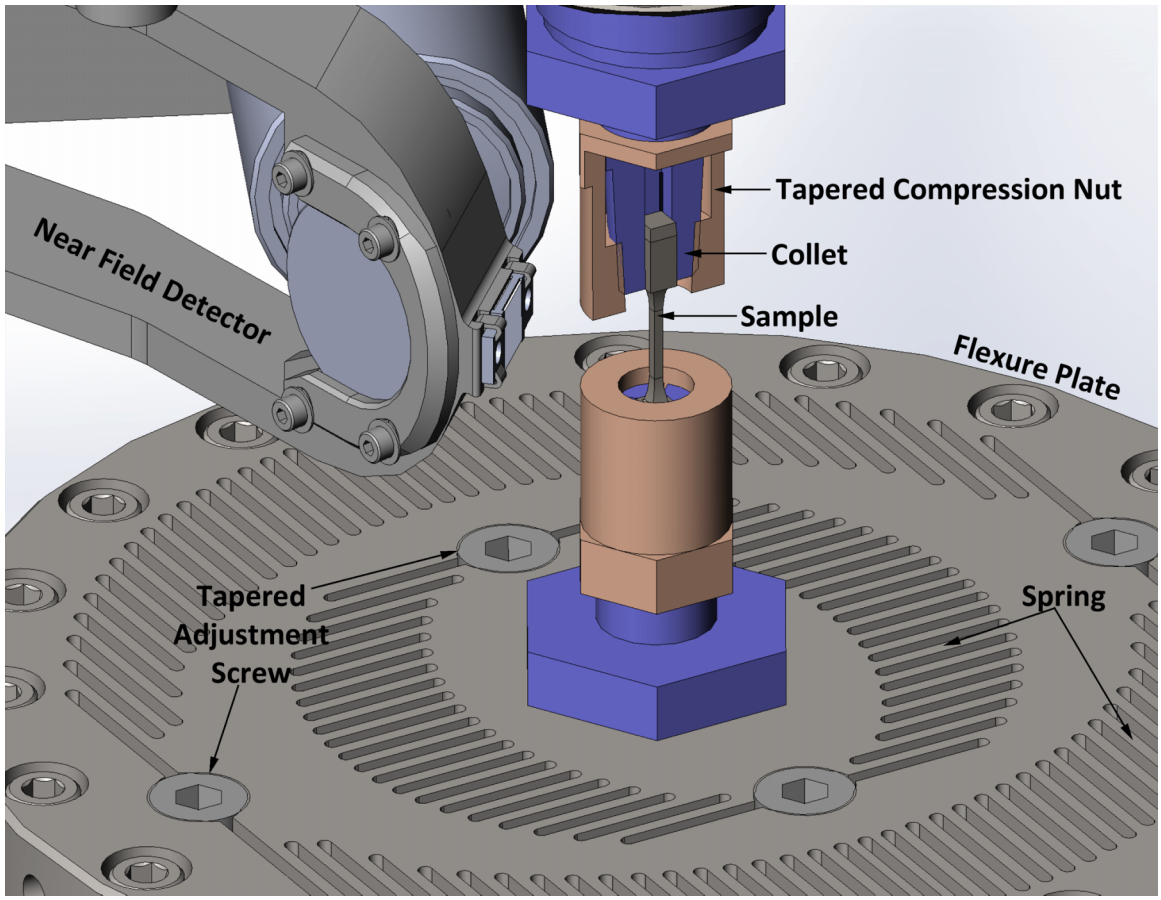

FIG. 3. Detailed schematic of the sample grips and lower flexure plate utilized in the RAMS load frame insert, with the upper grip shown in section view to reveal the internal details. The grips were designed to enable the near field detector, which is also shown, to be positioned as close as 5 mm from the sample. The flexure plates allow the upper and lower sample grips to be independently aligned to the rotation axis.

stiffness of 1300 N/μm in the adjustment directions and utilize the mechanical advantage of a tapered adjustment screw, as shown in Figure 3, to make the necessary adjustments to translate the centerline of the grips to be coaxial with the rotation axis. This resulted in approximately 1 μm of translational travel per 90° turn of the tapered adjustment screw. An alignment procedure that involved use of a dial indicator to monitor the position of a pin inserted into the grip during stage rotation was utilized. A best practice for achieving the finest sensitivity with this alignment procedure was found to be to slightly over-compensate with the initial correction, then subsequently repeat the procedure and make a relatively small correction in the opposing direction.

C. Minimalist grip design

A third major design constraint was to utilize a geometry that enabled the near field detector to sit as close as possible to the specimen during an experiment.[28] This required the development of sample grips with minimal radial dimensions. The grip design chosen is shown in Figure 3, where the near field detector is also shown for reference.

The sample grip design utilizes an interference fit, where a collet and tapered compression nut act to impart increasing pressure on the grip region of the specimen as increasing torque is applied to the tapered compression nut. The sample is held in place via friction, and therefore it is critical that the sample be fabricated within design tolerances in the grip region (±12.5 μm) and that clean sample and grip surfaces are maintained in order to be able to apply the full axial load (±2000 N) without sample slippage. Equally critical is the applied tightening torque of the tapered compression nut in order to provide the necessary gripping force. To address these concerns, we developed a motorized torque wrench with reaction force support for consistently and reliably installing and uninstalling samples in the RAMS device. The typical sample has a total length of 29 mm, a 1 mm × 1 mm cross section in the gage region, 8 mm gage length, and grip sections which are 3.2 mm × 3.2 mm in cross section and 6 mm in length. This grip design enabled the near field detector to be positioned as close as 5 mm downstream from the sample rotation axis.

III. APPLICATION

The RAMS device enables the concurrent application of various HEDM and tomographic techniques during *in situ* mechanical testing. We have utilized this capability to characterize a titanium alloy (Ti-7Al) tensile specimen undergoing room temperature deformation. A paper discussing these results in greater detail will be forthcoming, but we will introduce a portion of the experimental results as a means to highlight the capability of the RAMS device. The Ti-7Al material was processed to be a single phase (α, hexagonal close packed crystal structure) alloy with a basal texture and nearly equiaxed grains with an average size of ~100 μm. Due to its elastic and plastic anisotropy, the deformation behavior of this alloy is known to strongly depend on the local structure and loading state.[47–49] Therefore, the objective of this initial demonstration was to capture the intergranular stress heterogeneity that occurs upon loading of a bulk polycrystalline specimen.

A sample with an approximately 1.0×1.0 mm^2 gage region cross section and a gage length of 8 mm was installed in the RAMS load frame insert, and the initial structure was mapped with nf-HEDM, ff-HEDM, and μ-CT utilizing the experimental setup shown in Figure 1. The nf-HEDM data were collected using a 2 μm tall line-focused x-ray beam translated along ~200 μm of the specimen gage length to build up a measurement volume, whereas the ff-HEDM and μ-CT measurements were collected in single rotations using, respectively, a 600 μm and 1000 μm tall box beam which defined the volume. There was a small amount of axial load (23 MPa) on the sample for these initial measurements, which was a result of the specimen loading procedure (small axial translation of the tapered grips when tightening is unavoidable). The nf-HEDM measurements mapped the 3D grain structure with a spatial resolution of ~2 μm and a point-to-point orientation resolution of <0.1°. The μ-CT measurements confirmed that the specimen was initially free of voids or cracks above the spatial resolution of ~1.5 μm. The ff-HEDM measurements provided a centroid, crystallographic orientation, and grain-averaged full 3D elastic strain tensor for individual grains. Following these measurements of the initial state (load 0), the sample was subsequently loaded and ff-HEDM measurements were repeated at three different load levels (load 1, load 2, and load 3), where for each of these measurements, the sample was loaded slightly beyond the reported values and then immediately unloaded by 10% to the reported values in order to minimize the change in state of the sample during a ff-HEDM measurement due to stress relaxation[50] (the detector used limits the time for a full 360° scan with 0.25° rotation intervals to ~12 min). A macroscopic stress-strain curve indicating these measured load levels is shown in Figure 4, where a deviation from linearity at load 3 indicates the onset of plasticity. This is in agreement with the expectation of the development of a small degree of plasticity at stress levels below

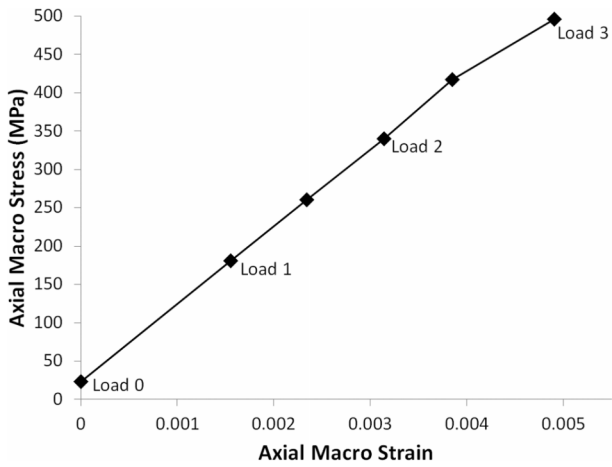

FIG. 4. Macroscopic stress-strain curve for an initial experiment utilizing the RAMS load frame insert. The four labeled loading states (load 0, load 1, load 2, and load 3) correspond to the HEDM measurements shown in Figures 5 and 6. Note that load 0, load 1, and load 2 correspond to elastic deformation only, whereas a small amount of plastic deformation has initiated at Load 3.

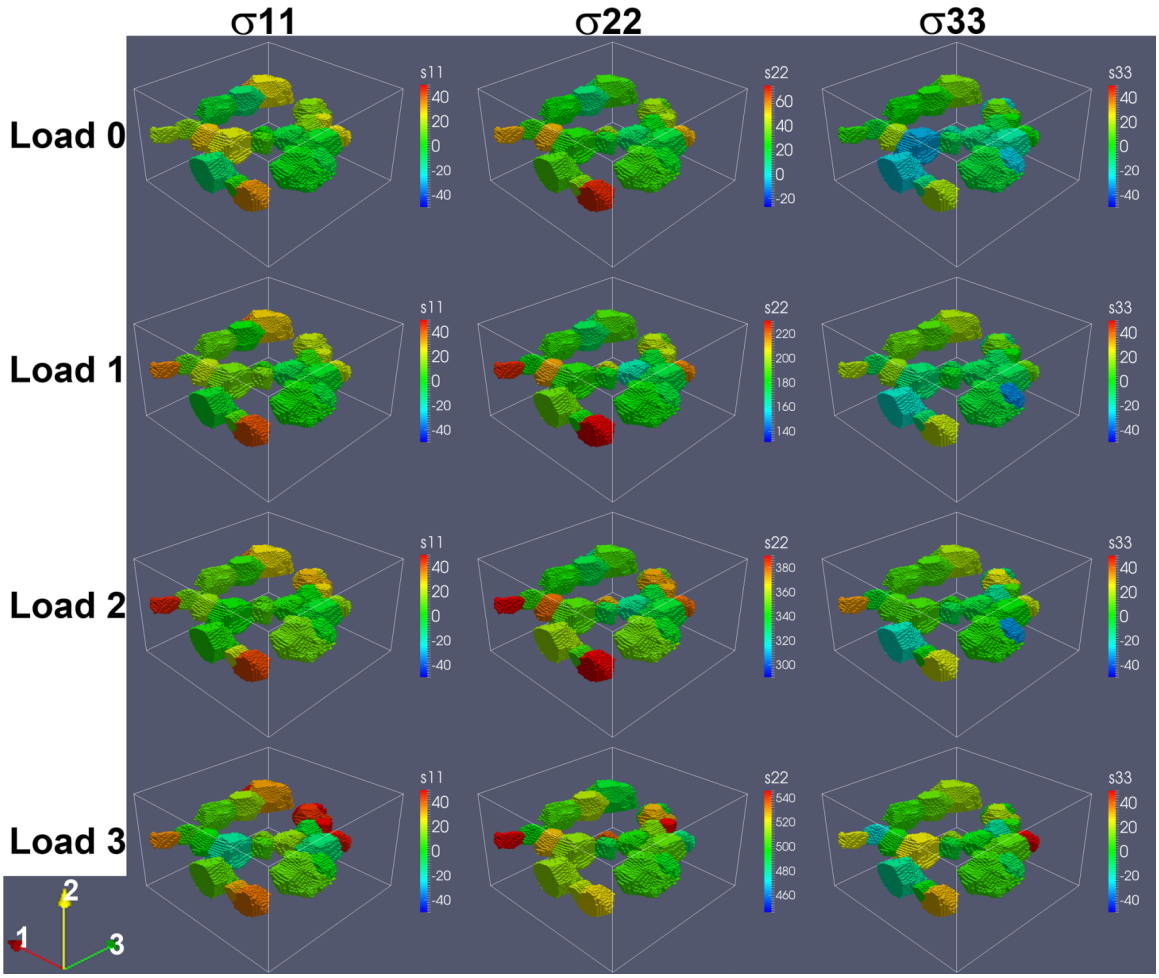

FIG. 5. 3D grain maps with overlaid normal stress components for a Ti-7Al tensile specimen measured with nf-HEDM and ff-HEDM using the experimental setup shown in Figure 1. In this figure, the data for 22 grains which were identified as good matches between the separate nf-HEDM and ff-HEDM datasets are shown. The tensile axis was 2, so that the macroscopic stress state $[\sigma_{11}\,\sigma_{22}\,\sigma_{33}\,\sigma_{12}\,\sigma_{13}\,\sigma_{23}]$ for loading states load 0, load 1, load 2, and load 3 was [0 23 0 0 0 0] MPa, [0 181 0 0 0 0] MPa, [0 340 0 0 0 0] MPa, and [0 496 0 0 0 0] MPa, respectively, as shown in Figure 4. Except for the σ_{22} cases, the color scales are the same for each map. Note that for certain grains, the σ_{22} values saturate above the applied macroscopic stress state.

the macroscopic yield stress of 600 MPa for this material. The macroscopic strain values in Figure 4 were calculated from two-point tracking[51] of surface feature displacements using optical images of the sample surface, i.e., two-point digital image correlation (DIC).

Combining nf-HEDM and ff-HEDM measurements, a grain centroid position tolerance of 20 μm and grain average orientation tolerance of 1° was utilized to register grains between the two techniques. Grains were identified in the nf-HEDM maps using a 1° voxel-to-voxel misorientation threshold. A cluster of 22 grains, with average centroid and orientation differences between the ff-HEDM and nf-HEDM data of 8.6 μm and 0.6°, respectively, were identified as the best matches and used for further analysis. Other measured grains may not have passed this tolerance test because they were only partially included in the irradiated measurement volume during one or the other of the non-concurrent HEDM measurements (recall that the nf-HEDM maps were collected over a 200 μm tall volume, whereas the ff-HEDM measurements were collected over a 600 μm tall volume).

The individual grain elastic strain tensors, as measured with ff-HEDM, were converted to stress tensors assuming the elastic properties of pure titanium.[52] Figures 5 and 6 show the individual normal and shear stress components, respectively, at the four different load levels overlaid on the 3D grain structures, as measured with nf-HEDM, for the 22 grains identified for further analysis. In these figures, the tensile axis is direction 2, so that the macroscopic σ_{22} values match those shown in Figure 4, while all other macroscopic stress components are zero. The uncertainty in the stress components is estimated to be approximately ±12 Mpa (assuming an elastic strain uncertainty of $\pm 10^{-4}$ and neglecting uncertainty in the elastic constants).[53]

From Figures 5 and 6, it can be seen that there is a significant degree of intergranular stress heterogeneity, which is seen to evolve with increasing load levels despite a minimal amount of plastic deformation. Of particular note are the noticeable changes in the distribution of grain level stress "hot spots." These local regions of high stress may be most favorable for critical phenomena such as void nucleation under continued deformation. The ability to quantify this heterogeneity and its evolution under mechanical processing *in situ* in an ensemble of grains represents a truly mesoscale measurement. The RAMS device is one of very few in the world that

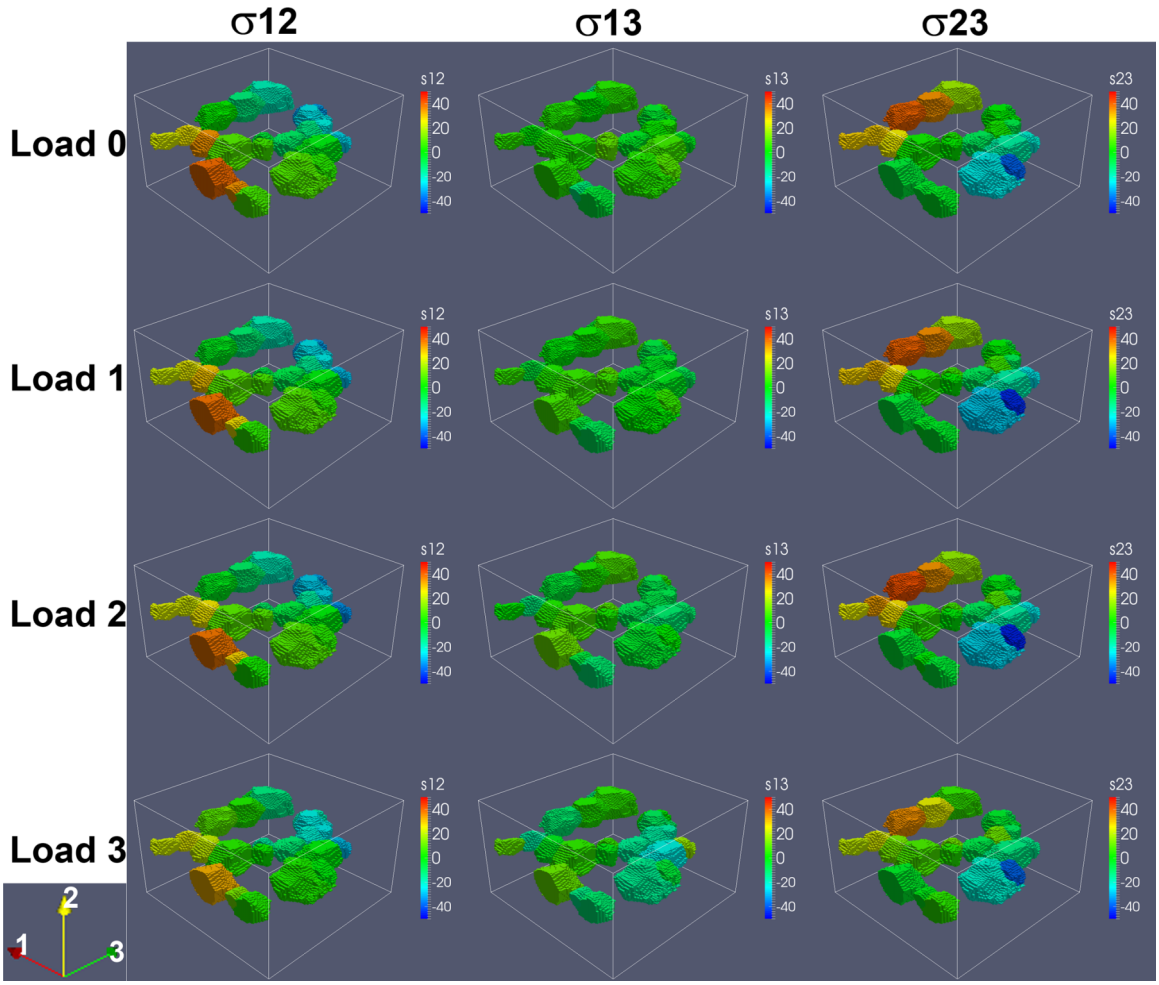

FIG. 6. 3D grain maps with overlaid shear stress components for the Ti-7Al tensile specimen shown in Figure 5, where the macroscopic load states correspond to Figure 4. The color scales are the same for each map.

facilitates these observations, and arguably the most accurate in terms of combined loading and positioning precision. The detailed analysis and comparison of this data to finite element simulations will be presented in a future paper. While only an example, this dataset demonstrates the great potential of HEDM/3DXRD methods for gaining insight into the mesoscale behavior of polycrystals. The multimodal, *in situ* data collection facilitated by the development of the RAMS device is a unique contribution to the field of experimental and applied science.

IV. SUMMARY

We have described the development of the so-called RAMS load frame insert. This device will enable the concurrent application of various high energy x-ray characterization techniques which require specimen rotation, such as HEDM/3DXRD and tomography while conducting *in situ* mechanical testing experiments. This capability may provide critical data for the development and validation of microstructure sensitive materials models. In a first application, we collected ff-HEDM, nf-HEDM, μ-CT, and DIC data during an *in situ* tension test of a Ti-7Al sample and presented intergranular stress results that display marked stress heterogeneity. We expect that the device will be useful in future studies of a variety of materials under various loading conditions and utilizing an array of HEDM/3DXRD measurement techniques. Future versions of the device include a standalone RAMS load frame being developed at the Cornell High Energy Synchrotron Source and a high load capacity standalone RAMS load frame being developed at APS.

ACKNOWLEDGMENTS

The authors would like to thank Dr. Adam Pilchak (Air Force Research Laboratory) for providing the Ti-7Al material examined in this study, Dr. Chris Woodward (Air Force Research Laboratory) for help securing the computational resources required for the data reduction, Ali Mashayekhi (Advanced Photon Source) and Erika Benda (Advanced Photon Source) for help with the experimental setup, and Dr. Dennis Dimiduk (Air Force Research laboratory) and Professor Matthew Miller (Cornell University) for useful discussions. The authors acknowledge support from the Materials & Manufacturing Directorate of the U.S. Air Force Research Laboratory. Use of the Advanced Photon Source, an Office of Science User Facility operated for the U.S. Department of Energy (DOE) Office of Science by Argonne

National Laboratory was supported by the U.S. DOE under Contract No. DEAC02-06CH11357.

[1]P. R. Dawson, Int. J. Solids Struct. **37**, 115 (2000).
[2]F. Roters, P. Eisenlohr, L. Hantcherli, D. D. Tjahjanto, T. R. Bieler, and D. Raabe, Acta Mater. **58**, 1152 (2010).
[3]D. L. McDowell, J. H. Panchal, H. J. Choi, C. C. Seepersad, J. K. Allen, and F. Mistree, *Integrated Design of Multiscale, Multifunctional Materials and Products* (Butterworth-Heinemann, Burlington, MA, 2010).
[4]*Computational Methods for Microstructure-Property Relationships*, edited by S. Ghosh and D. Dimiduk (Springer, New York, 2011).
[5]R. Pokharel, J. Lind, A. K. Kanjarla, R. A. Lebensohn, S. F. Li, P. Kenesei, R. M. Suter, and A. D. Rollett, Annu. Rev. Condens. Matter Phys. **5**, 317 (2014).
[6]J. C. Schuren, P. A. Shade, J. V. Bernier, S. F. Li, B. Blank, J. Lind, P. Kenesei, U. Lienert, R. M. Suter, T. J. Turner, D. M. Dimiduk, and J. Almer, Curr. Opin. Solid State Mater. Sci. **19**, 235 (2015).
[7]G. Winther, L. Margulies, S. Schmidt, and H. F. Poulsen, Acta Mater. **52**, 2863 (2004).
[8]S. R. Kalidindi, A. Bhattacharyya, and R. D. Doherty, Proc. R. Soc. A **460**, 1935 (2004).
[9]A. Musienko, A. Tatschl, K. Schmidegg, O. Kolednik, R. Pippan, and G. Cailletaud, Acta Mater. **55**, 4121 (2007).
[10]E. Heripre, M. Dexet, J. Crepin, L. Gelebart, A. Roos, M. Bornert, and D. Caldemaison, Int. J. Plast. **23**, 1512 (2007).
[11]Z. Zhao, M. Ramesh, D. Raabe, A. M. Cuitino, and R. Radovitzky, Int. J. Plast. **24**, 2278 (2008).
[12]L. St-Pierre, E. Heripre, M. Dexet, J. Crepin, G. Bertolino, and N. Bilger, Int. J. Plast. **24**, 1516 (2008).
[13]A. J. Beaudoin, M. Obstalecki, R. Storer, W. Tayon, J. Mach, P. Kenesei, and U. Lienert, Modell. Simul. Mater. Sci. Eng. **20**, 024006 (2012).
[14]P. A. Shade, M. A. Groeber, J. C. Schuren, and M. D. Uchic, Integr. Mater. Manuf. Innov. **2**, 5 (2013).
[15]T. J. Turner, P. A. Shade, J. C. Schuren, and M. A. Groeber, Modell. Simul. Mater. Sci. Eng. **21**, 015002 (2013).
[16]H. Lim, J. D. Carroll, C. C. Battaile, T. E. Bucheit, B. L. Boyce, and C. R. Weinberger, Int. J. Plast. **60**, 1 (2014).
[17]C. C. Tasan, M. Diehl, D. Yan, C. Zambaldi, P. Shanthraj, F. Roters, and D. Raabe, Acta Mater. **81**, 386 (2014).
[18]M. P. Miller and P. R. Dawson, Curr. Opin. Solid State Mater. Sci. **18**, 286 (2014).
[19]C. Zhang, H. Li, P. Eisenlohr, W. Liu, C. J. Boehlert, M. A. Crimp, and T. R. Bieler, Int. J. Plast. **69**, 21 (2015).
[20]H. Abdolvand, M. Majkut, J. Oddershede, S. Schmidt, U. Lienert, B. J. Diak, P. J. Withers, and M. R. Daymond, Int. J. Plast. **70**, 77 (2015).
[21]H. F. Poulsen, *Three-Dimensional X-Ray Diffraction Microscopy: Mapping Polycrystals and their Dynamics* (Springer, Berlin, 2004).
[22]U. Lienert, S. F. Li, C. M. Hefferan, J. Lind, R. M. Suter, J. V. Bernier, N. R. Barton, M. C. Brandes, M. J. Mills, M. P. Miller, B. Jakobsen, and W. Pantleon, JOM **63**, 70 (2011).
[23]H. F. Poulsen, J. Appl. Crystallogr. **45**, 1084 (2012).
[24]H. F. Poulsen, S. F. Nielsen, E. M. Lauridsen, S. Schmidt, R. M. Suter, U. Lienert, L. Margulies, T. Lorentzen, and D. J. Jensen, J. Appl. Crystallogr. **34**, 751 (2001).
[25]L. Margulies, T. Lorentzen, H. F. Poulsen, and T. Leffers, Acta Mater. **50**, 1771 (2002).
[26]J. Oddershede, S. Schmidt, H. F. Poulsen, H. O. Sorensen, J. Wright, and W. Reimers, J. Appl. Crystallogr. **43**, 539 (2010).
[27]J. V. Bernier, N. R. Barton, U. Lienert, and M. P. Miller, J. Strain Anal. Eng. Des. **46**, 527 (2011).
[28]R. M. Suter, D. Hennessy, C. Xiao, and U. Lienert, Rev. Sci. Instrum. **77**, 123905 (2006).
[29]S. F. Li and R. M. Suter, J. Appl. Crystallogr. **46**, 512 (2013).
[30]P. J. Withers and M. Preuss, Annu. Rev. Mater. Res. **42**, 81 (2012).
[31]B. E. Blank, J. Schuren, P. Shade, and T. Turner, U.S. patent application 14/461,582 (18 August 2014).
[32]T. M. Breunig, S. R. Stock, and R. C. Brown, Mater. Eval. **51**, 596 (1993).
[33]H. G. Brokmeier, U. Zink, T. Reinert, and W. Murach, J. Appl. Crystallogr. **29**, 501 (1996).
[34]J. C. Schuren, M. P. Miller, and A. Kazimirov, Exp. Mech. **52**, 461 (2012).
[35]H. A. Bale, A. Haboub, A. A. MacDowell, J. R. Nasiatka, D. Y. Parkinson, B. N. Cox, D. B. Marshall, and R. O. Ritchie, Nat. Mater. **12**, 40 (2013).
[36]S. F. Li, J. Lind, C. M. Hefferan, R. Pokharel, U. Lienert, A. D. Rollett, and R. M. Suter, J. Appl. Crystallogr. **45**, 1098 (2012).
[37]J. Lind, S. F. Li, R. Pokharel, U. Lienert, A. D. Rollett, and R. M. Suter, Acta Mater. **76**, 213 (2014).
[38]H. M. Reiche, S. C. Vogel, P. Mosbrucker, E. J. Larson, and M. R. Daymond, Rev. Sci. Instrum. **83**, 053901 (2012).
[39]M. Hoelzel, W. M. Gan, M. Hofmann, C. Randau, G. Seidl, Ph. Juttner, and W. W. Schmahl, Nucl. Instrum. Methods Phys. Res., Sect. A **711**, 101 (2013).
[40]P. Wyss, P. Thurner, R. Bronnimann, U. Sennhauser, M. Stampanoni, R. Abela, and R. Muller, Rev. Sci. Instrum. **76**, 076106 (2005).
[41]W. Xu, K. Lauer, Y. Chu, and E. Nazaretski, J. Synchrotron Radiat. **21**, 1367 (2014).
[42]H. Sharma, R. M. Huizenga, and S. E. Offerman, J. Appl. Crystallogr. **45**, 705 (2012).
[43]D. H. Lassila, M. M. LeBlanc, and G. J. Kay, J. Eng. Mater. Technol. **124**, 290 (2002).
[44]P. A. Shade, R. Wheeler, Y. S. Choi, M. D. Uchic, D. M. Dimiduk, and H. L. Fraser, Acta Mater. **57**, 4580 (2009).
[45]R. V. Jones and I. R. Young, J. Sci. Instrum. **33**, 11 (1956).
[46]C. Wenjie, L. Wei, and Y. Guilin, in *11th International Conference on Control Automation Robotics Vision* (IEEE, 2010), p. 1755.
[47]U. Lienert, M. C. Brandes, J. V. Bernier, J. Weiss, S. D. Shastri, M. J. Mills, and M. P. Miller, Mater. Sci. Eng. A **524**, 46 (2009).
[48]M. C. Brandes, M. J. Mills, and J. C. Williams, Metall. Mater. Trans. A **41**, 3463 (2010).
[49]J. Kwon, M. C. Brandes, P. Sudharshan Phani, A. P. Pilchak, Y. F. Gao, E. P. George, G. M. Pharr, and M. J. Mills, Acta Mater. **61**, 4743 (2013).
[50]P. Dawson, D. Boyce, S. MacEwen, and R. Rogge, Metall. Mater. Trans. A **31**, 1543 (2000).
[51]M. Guizar-Sicairos, S. T. Thurman, and J. R. Fienup, Opt. Lett. **33**, 156 (2008).
[52]E. S. Fisher and C. J. Renkin, Phys. Rev. **135**, 482 (1964).
[53]J. C. Schuren and M. P. Miller, J. Strain Anal. Eng. Des. **46**, 663 (2011).